476 *Chem. Mater.* **2010,** *22,* 476–481
DOI:10.1021/cm9031946

CHEMISTRY OF MATERIALS
Article

Nanosphere Lithography at the Gas/Liquid Interface: A General Approach toward Free-Standing High-Quality Nanonets

Cheng Li, Guosong Hong, and Limin Qi*

Beijing National Laboratory for Molecular Sciences (BNLMS), State Key Laboratory for Structural Chemistry of Unstable and Stable Species, College of Chemistry, Peking University, Beijing 100871, People's Republic of China

Received October 16, 2009. Revised Manuscript Received November 21, 2009

A general nanosphere lithography (NSL) approach toward facile fabrication of free-standing, large-area, high-quality nanonets was developed, which was based on a floating colloidal crystal monolayer (CCM) mask at the gas/liquid interface for materials deposition via interfacial reactions. The hole size, spacing, and thickness of the highly ordered nanonets, which showed interesting photonic properties, can be readily adjusted. This NSL approach at the gas/liquid interface can be easily extended to fabricate large-area ordered nanonets of various metal sulfides, metals as well as inorganic minerals. Furthermore, a variety of ordered gold nanoarrays with unusual patterns were produced by using nanonet bilayers as unique deposition masks, suggesting that the obtained transferable, high-quality nanonets can function as versatile lithographic masks to generate novel nanopatterns.

The technical development of nanofabrication is driven by the demand of miniaturization of device features with improved performance and decreased cost in the electronic and information industry and would provide new opportunities for fundamental research in low dimensional physics.[1,2] The realization of patterning of useful level in nanofabrication requires lithography techniques to become more convenient, cost-effective, productive, and compatible with various materials. Nanoholes periodically patterned in a continuous thin film of metals, semiconductors, or dielectrics often lead to unusual properties due to scattering of electromagnetic wave on the subwavelength scale.[3−5] Ordered nanonets could also provide useful masks for the fabrication of patterned nanoarrays or novel nanoobjects. Moreover, nano/microsieves with monodisperse pores and high pore density are desirable as high-performance nano/microfiltration membranes.[6,7] To fabricate such regular porous membranes, focused ion-beam milling of a preformed thin film,[3,4] physical deposition, or etching through masks patterned by poly(dimethylsiloxane) (PDMS) stamps,[8] electron-beam lithography,[9] or laser interference holography,[6,7] and chemical deposition by templating against anodic aluminum oxide[5,10] have been successfully used. However, of these strategies, few combine generality and simplicity for the production of large-area, highly ordered nanonets.

Nanosphere lithography (NSL) that usually employs hexagonal-close-packed (hcp) colloidal crystal monolayers (CCMs) as masks has been proven to be a flexible and cost-effective technique to fabricate nanostructured arrays with long-range periodicity in a large scale.[11−14] Through-pored films can be produced by filling the voids in CCMs through sol/solution deposition,[15,16] electro- or electroless deposition[17,18] or by trapping particles within polymer films;[19] however, the thus formed films tend to have interconnected pore structures and a thickness larger than the pore radius. To avoid this problem, multistep replication has been

*To whom correspondence should be addressed. E-mail: liminqi@pku.edu.cn. Fax: +86-10-62751708.

(1) Gates, B.; Xu, Q.; Stewart, M.; Ryan, D.; Willson, C.; Whitesides, G. *Chem. Rev.* **2005**, *105*, 1171.
(2) Henzie, J.; Barton, J.; Stender, C.; Odom, T. *Acc. Chem. Res.* **2006**, *39*, 249.
(3) Ebbesen, T.; Lezec, H.; Ghaemi, H.; Thio, T.; Wolff, P. *Nature* **1998**, *391*, 667.
(4) Gordon, R.; Sinton, D.; Kavanagh, K.; Brolo, A. *Acc. Chem. Res.* **2008**, *41*, 1049.
(5) Liao, Q.; Wang, Y.; Li, J.; Wu, K.; Ai, X.; Zhang, J. *Appl. Phys. Lett.* **2007**, *91*, 041103.
(6) Kuiper, S.; van Rijn, C.; Nijdam, W.; Elwenspoek, M. *J. Membr. Sci.* **1998**, *150*, 1.
(7) Prenen, A.; van der Werf, J.; Bastiaansen, C.; Broer, D. *Adv. Mater.* **2009**, *21*, 1751.
(8) Henzie, J.; Lee, M.; Odom, T. *Nat. Nanotechnol.* **2007**, *2*, 549.
(9) Wang, Y.; Wu, K. *J. Am. Chem. Soc.* **2005**, *127*, 9986.
(10) Henzie, J.; Barton, J.; Stender, C.; Odom, T. *Acc. Chem. Res.* **2006**, *39*, 249.
(11) (a) Hulteen, J.; van Duyne, R. *J. Vac. Sci. Technol., A* **1995**, *13*, 1. (b) Zhang, X.; Whitney, A.; Zhao, J.; Hicks, E.; van Duyne, R. *J. Nanosci. Nanotechnol.* **2006**, *6*, 1.
(12) (a) Yang, S.; Jang, S.; Choi, D.; Kim, S.; Yu, H. *Small* **2006**, *2*, 458. (b) Jiang, P. *Angew. Chem., Int. Ed.* **2004**, *43*, 5625. (c) Acikgoz, C.; Ling, X. Y.; Phang, I. Y.; Hempenius, M. A.; Reinhoudt, D. N.; Huskens, J.; Vancso, G. *J. Adv. Mater.* **2009**, *21*, 2064.
(13) Li, Y.; Cai, W.; Duan, G. *Chem. Mater.* **2008**, *20*, 615.
(14) Zhang, G.; Wang, D. *Chem. Asian J.* **2009**, *4*, 236.
(15) Cho, Y.; Cho, G.; Lee, J. *Adv. Mater.* **2004**, *16*, 1814.
(16) (a) Sun, F.; Cai, W.; Li, Y.; Cao, B.; Lei, Y.; Zhang, L. *Adv. Funct. Mater.* **2004**, *14*, 283. (b) Sun, F.; Cai, W.; Li, Y.; Jia, L.; Lu, F. *Adv. Mater.* **2005**, *17*, 2872.
(17) (a) Bartlett, P.; Baumberg, J.; Coyleb, S.; Abdelsalam, M. *Faraday Discuss.* **2004**, *125*, 117. (b) Abdelsalam, M.; Bartlett, P.; Baumberg, J.; Coyle, S. *Adv. Mater.* **2004**, *16*, 90.
(18) (a) Cong, H.; Cao, W. *Adv. Funt. Mater.* **2005**, *15*, 1821. (b) Fu, M.; Zhou, J.; Li, B.; Huang, X.; Wang, Y.; Li, L. *J. Mater. Chem.* **2008**, *18*, 5986.
(19) Jang, S.; Choi, D.; Heo, C.; Lee, S.; Yang, S. *Adv. Mater.* **2008**, *20*, 4862.

Published on Web 12/21/2009

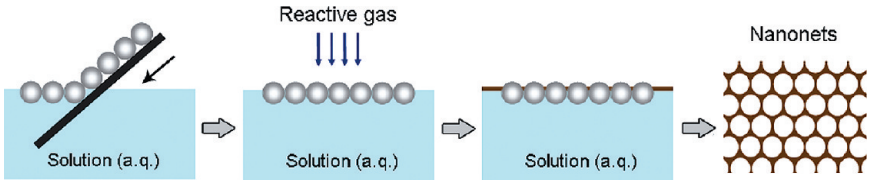

Figure 1. Schematic illustration of the fabrication of free-standing high-quality nanonets by nanosphere lithography at the gas/liquid interface.

conducted, yet leading to porous thin films with poor regularity.[20] As an alternative route, nonclose-packed (ncp) CCMs have been used as the deposition mask to produce periodic nanohole arrays.[21,22] Nevertheless, laborious processes such as polymerization after spin-coating or plasma etching were required to generate ncp CCM masks for subsequent metal deposition on solid substrates, resulting in metal nanonets attached to the substrate with limited transferability. Moreover, the materials that have been produced with CCMs are mostly limited to metals and metal oxides. Therefore, it remains a great challenge to develop general methods to fabricate high-quality nanonets with both excellent transferability and compositional diversification.

Herein we report on a very simple and straightforward NSL approach to fabricate large-area free-standing nanonets with high regularity at the gas/liquid interface by using the floating CCM at a solution surface[16,23,24] as the mask for the interfacial material deposition via gas/liquid interface reactions. The gas/liquid interface can provide a two-dimensionally (2D) constrained environment and has long been exploited to prepare inorganic films via reactive gas diffusion. The development of porous thin film via colloidal monolayer templating at liquid−gas interface was first reported by Geodel et al.;[25] however, a long-range order was generally lacking for the obtained porous thin films since colloidal sphere monolayers with relatively low regularity were employed as template. In the present work, we develop a novel colloidal lithography technique by employing floating CCM mask with high regularity at a solution surface to fabricate large-area, high-quality nanonets of various inorganic materials including metal sulfides, metals, and inorganic minerals. Figure 1 shows schematically a process flow outlining the major steps leading to the formation of free-standing nanonets. First, an hcp CCM film was assembled on a solid substrate,[26] which was then released onto the reactant solution surface by inserting the substrate into a subphase containing the reactant ions. As a result of the action of capillary force enhanced by every three adjacent spheres of the CCM,[16a,23] the floating CCM was partially immersed with the solution surface lying above its tangent-point plane, thus generating a periodically exposed solution surface that masked equivalently by a nonclose-packed nanodisk array. Second, a reactive gas atmosphere was introduced to initiate the interfacial reaction with the subphase. The material deposition occurred initially at the solution surface rather than at the supporting substrates like in most colloidal templating methods. Finally, a sheet of intact nanonet was obtained after a proper period of reaction by dissolving away the CCM mask. The floating state of the nanonets allows their convenient transfer onto any solid substrate, including holey ones. This approach provides a facile total-chemical procedure that is compatible with a variety of materials and can be carried out at room temperature without any special equipment.

Experimental Section

Assembly of CCMs at Solution Surface. First, the colloidal crystal monolayer (CCM) film was fabricated on a silicon substrate using a method recently developed at our lab.[26] In brief, 10−14 μL water/ethanol dispersion containing monodisperse polystyrene (PSt) or poly(styrene-methyl methacrylate-acrylic acid) (P(St-MMA-AA)) colloidal spheres was dropped onto the top surface of a 1 × 1 cm piece of glass surrounded by water located at the midbottom of a Petri dish. The dispersion spread freely on the water surface until it covered nearly the whole surface area, resulting in a colorful CCM film up to ~16 cm^2 in area. Then the CCM film was picked up with a silicon plate with a specific size and shape (typically, a square ~1 cm^2 in area) and transferred onto the surface of aqueous reactant solutions by inserting the plate into the solution with an inclining angle. It may be noted that the CCM film was not directly assembled on the surface of aqueous reactant solutions from colloidal spheres, but was first assembled on the surface of water without reactant ions, which was then picked up by a silicon plate and then transferred onto the surface of specific aqueous reactant solutions. Our preliminary experiments showed that if the water/ethanol dispersion of colloidal spheres was directly dispersed on the surface of aqueous reactant solutions (e.g., 10 mM), it spread much more quickly, possibly due to the effects of the electrolytes on the interfacial tension between the colloidal dispersion and water, resulting in the formation of CCM films with bad ordering. Therefore, the current method avoided the effects of reactant ions on the assembly of CCM films, thereby enabling the preparation of large-area, high-quality CCM films.

Preparation of Nanonets by NSL at the Gas/Liquid Interface. In a typical synthesis of Ag_2S nanonets, a vessel containing 5 mL of 10 mM $AgNO_3$ aqueous solution with a piece of floating CCM was covered by Parafilm punched with one aperture and placed in a closed desiccator where one vial containing 1.0 g thioacetamide (TAA) powder and another containing 1.5 mL of 7 M nitric acid were placed separately, slowly generating H_2S gas to initiate the interfacial reaction with silver ions (Scheme S1, Supporting Information (SI). *Caution! H_2S is virulent*). Experimental parameters for the fabrication of nanonets of

(20) Xu, H.; Goedel, W. *Small* **2005**, *1*, 808.
(21) Jiang, P.; McFarland, M. *J. Am. Chem. Soc.* **2005**, *127*, 3710.
(22) Liu, X.; Sun, C.-H.; Linn, N. C.; Jiang, B.; Jiang, P. *J. Phys. Chem. C* **2009**, *113*, 14804.
(23) Sun, F.; Yu, J. *Angew. Chem., Int. Ed.* **2007**, *46*, 773.
(24) Li, Y.; Lee, E.; Cho, S. *J. Phys. Chem. C* **2007**, *111*, 14813.
(25) (a) Xu, H.; Goedel, W. A. *Langmuir* **2002**, *18*, 2363. (b) Yan, F.; Goedel, W. A. *Chem. Mater.* **2004**, *16*, 1622. (c) Xu, H.; Goedel, W. A. *Angew. Chem., Int. Ed.* **2003**, *42*, 4694.
(26) Li, C.; Hong, G.; Wang, P.; Yu, D.; Qi, L. *Chem. Mater.* **2009**, *21*, 891.

other inorganic materials were summarized in SI Table S1). All these experiments were carried at room temperature. After reaction at room temperature for certain periods the CCMs were dissolved away with dichloromethane and nanonets were picked up from the solution surface by certain substrates.

Fabrication of Au Nanoparticle Arrays Using Nanonets As Deposition Masks. The Ag_2S nanonet bilayers were constructed on Si substrate in a layer-by-layer manner, which was realized simply by picking up monolayer nanonets sequentially from the solution surface with a same substrate. Since the formed Ag_2S nanonet film adopted a shape of square, the relative rotational angles between two layers of nanonets could be adjusted by carefully changing the rotational angle of the Si substrate coated with a single layer of Ag_2S nanonet film with respect to the floating Ag_2S nanonet film. However, it was still difficult to achieve an accurate control over the translational distance and relative rotational angles between two layers of nanonets by this simple manual process, which may require further efforts involving micromanipulation. Monolayer or bilayer Ag_2S nanonets on the silicon substrate were mounted in a thermal evaporator (ZHD-400, Beijing Technol Science Co., Ltd., 10^{-5} Pa), where a 50 nm-thick Au (99.99%) layer was deposited on the nanonet mask. Subsequently, the nanonet mask was lifted off using adhesive tapes, leaving behind Au nanopatterns on the substrate.

Characterization. The samples were characterized by scanning electron microscopy (SEM, Hitachi FE-S4800, 2 kV), transmission electron microscopy (TEM, JEOL JEM200CX, 160 kV), and XRD (RigakuD/ MAX-PC2500, Cu Kα). Optical transmission spectra were recorded with normal incidence using a Perkin-Elmer Lambda 950 UV/vis/NIR spectrometer.

Calculation of Stop Band Positions. To determine the stop band position of the obtained Ag_2S nanonets, we adopt a simplified model for 2D arrays,[27] in which the first-order diffracted waves with wavevector $k(\omega)$ can couple to photonic modes of the lattice if $k(\omega) = n_{\text{eff}} \cdot 2\pi/\lambda = G_{\text{mm}}$, where n_{eff} is the effective refractive index and G_{mm} is the reciprocal lattice vector. For the current hexagonally patterned Ag_2S nanonets, $G_{\text{mm}} = \frac{4\pi}{\sqrt{3}D} \cdot \sqrt{m^2 + n^2 + mn}$, where D is the particle diameter of CCM. Then, the smallest reciprocal lattice vector is $G_{1,0} = \frac{4\pi}{\sqrt{3}D}$. Therefore, the transmission dip (λ_d), that is, the stop band position, can be calculated by the formula $\lambda_d = \frac{\sqrt{3}D \cdot n_{eff}}{2}$. During the calculation, n_{eff} was obtained by using a crude effective medium estimation, $n_{\text{eff}} = (n^2_{Ag_2S} f_{Ag_2S} + n^2_{\text{air}}(1-f_{Ag_2S}))^{1/2}$, where $n_{\text{air}} = 1$, $n_{Ag_2S} = \sqrt{\varepsilon} = 2.97$,[28] and f_{Ag_2S} is the volume fraction of Ag_2S in this thin films, which was calculated from the hole diameter d and sphere diameter D (SI Scheme S2).

Results and Discussion

As a representative demonstration, the production of high-quality Ag_2S nanonets will be discussed in detail. A complete sheet of Ag_2S nanonet with an area ~ 1 cm^2 can be readily obtained on a solid substrate (SI Figure S1). Figure 2a shows a low-magnification SEM image of a sheet of Ag_2S nanonet obtained with a CCM mask consisting of 500 nm-diameter polystyrene (PSt) spheres after 24 h of reaction and suspended freely on a copper grid with 0.1 mm-holes. A zoom-in SEM image shown in Figure 2b reveals that the nanonet has highly ordered, hexagonally packed circular holes that inherited from the original CCM mask. Figure 2c shows a further enlarged SEM image of the nanonet settled on a silicon substrate, which suggests a uniform hole diameter of 400 nm and a bar width of around 100 nm. Compared with the diameter of the mask spheres, the as-grown nanonet has a smaller hole size as a consequence of a slightly higher front of material deposition than the tangent-point plane of the CCM mask. A perspective view of the nanonet presented in Figure 2d shows that the nanonet has a 2D flat net-like structure with a film thickness $\sim$100 nm, significantly distinguishing itself from the 3D interconnected bowl-shaped arrays usually obtained by CCM templating. Figure 2e shows a typical TEM image of the nanonet and the corresponding selected-area electron diffraction (SAED) pattern, indicating that the nanonet is composed of polycrystalline α-Ag_2S, which is further confirmed by powder X-ray diffraction (XRD) and high resolution TEM (HRTEM) (SI Figure S2). A free-standing nanonet folded during sample preparation is shown in Figure 2f, which demonstrates its remarkable flexibility and therefore its compatibility with nonplanar surfaces. The obtained Ag_2S nanonet thin film was further characterized by atomic force microscopy (AFM) and the related section analysis indicated that the film thickness was 100 ± 10 nm (SI Figure S3), which is in good agreement with the SEM observation. The hole diameter and thus the hole spacing of the nanonets can be readily adjusted

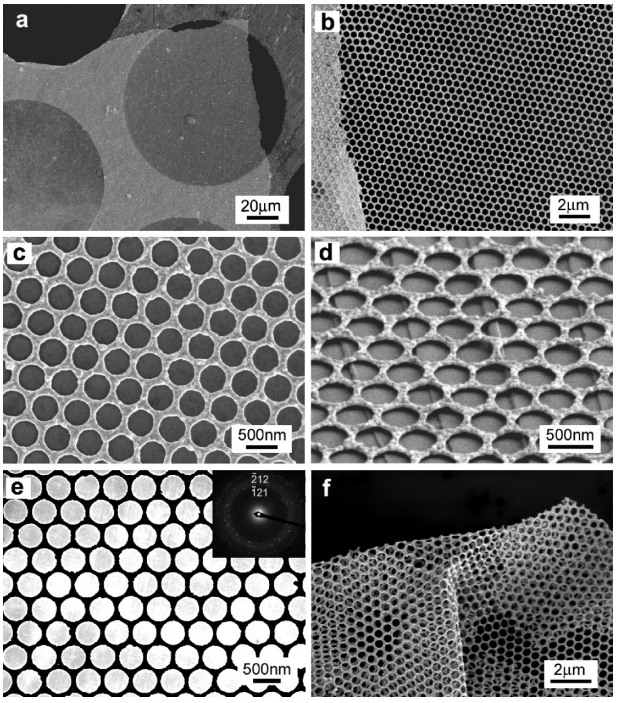

Figure 2. SEM images of Ag_2S nanonets suspended on a holey copper grid (a, b), on a flat silicon plate (c), and on a silicon plate with terraces (d). (e) TEM image and SAED pattern (inset) of Ag_2S nanonet. (f) SEM image of free-standing nanonet folded during sample preparation.

(27) (a) Landstrom, L.; Brodoceanu, D.; Arnold, N.; Piglmayer, K.; Bauerle, D. *Appl. Phys. A: Mater. Sci. Process.* **2005**, *81*, 911. (b) Gao, Y.; Li, A. D.; Gu, Z. B.; Wang, Q. J.; Zhang, Y.; Wu, D.; Chen, Y. F.; Ming, N. B.; Ouyang, S. X.; Yu, T. *Appl. Phys. Lett.* **2007**, *91*, 031910.

(28) Hsu, T. Y.; Buhay, H.; Murarka, N. P. *SPIE Millimeter Opt.* **1980**, *259*, 38.

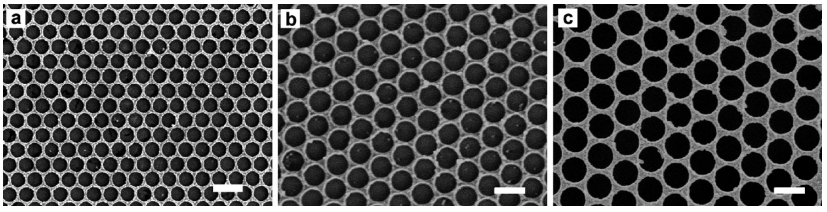

Figure 3. SEM images of Ag_2S nanonets prepared with floating CCMs of different particle diameters as masks: (a) 600 nm, (b) 800 nm, (c) 1000 nm. All the scale bars are 1 μm.

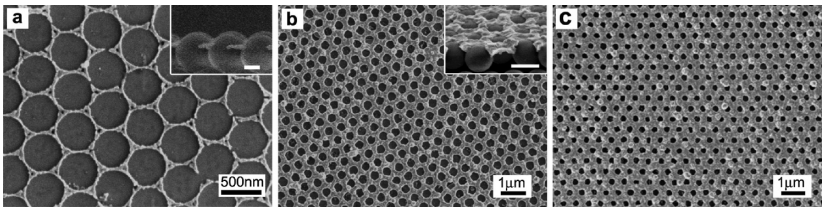

Figure 4. SEM images Ag_2S nanonets obtained at different reaction periods: (a) 12 h, (b) 48 h, (c) 108 h. Insets of (a) and (b) show the corresponding cross-sectional images of the Ag_2S-PSt composite films and the scale bars are 200 and 500 nm, respectively.

by using CCMs with different particle diameters as the floating mask under otherwise identical conditions. As shown in Figure 3, Ag_2S nanonets with holes of 470, 670, and 800 nm in diameter were obtained by using CCMs with particle diameters of 600 nm, 800 nm, and 1 μm as masks, respectively.

To investigate the growth process of the nanonets, the products obtained by using a CCM mask consisting of 500 nm-diameter PSt spheres were harvested at different reaction periods (Figure 4). A shorter reaction time (i.e., 12 h) led to the formation of an incomplete net-like structure consisting of arrays of connected nanorings (Figure 4a). The triangular voids among the nanorings suggest that the material deposition started at the gas−liquid−solid interface, that is, on the circular lines where polymer sphere surface met the water surface, which were higher than the tangent-point plane of the CCM mask due to the capillary ascent at the three-phase interface. The corresponding cross-sectional SEM image of the Ag_2S-PSt composite film confirmed that the line of materials deposition was actually higher than the tangent-point plane of the CCM mask. The triangular voids were subsequently fully filled with Ag_2S particles by continuous gas-solution reactions until an integrated nanonet formed at 24 h, as shown in Figure 2. With increasing reaction time to 48 h, the primary Ag_2S particles constituting the nanonets became larger and gradually grew toward the PSt spheres and into the gas phase (Figure 4b). Further elongation of the reaction period to 108 h resulted in a significant shrinkage of the hole size accompanied by an increase in both the bar thickness and the film thickness (Figure 4c).

As a result of a 2D periodic change of refractive index caused by the hexagonally ordered nanohole arrays within a continuous thin film, the as-prepared Ag_2S nanonets demonstrated intensive structural colors (SI Figure S1). Although various films with 2D ordered structures have been constructed using NSL, only a few reports concerned about their photonic properties,[29,30] which may enable them to function as thin film optical sensors. Here the photonic properties of the Ag_2S nanonets were carefully investigated by measuring their optical transmission spectra. With normal-incidence, the transmission spectra of all the Ag_2S nanonets prepared with CCMs of different particle diameters showed sharp transmission dips (i.e., stop bands), whereas the spectrum of unstructured Ag_2S film grown in the absence of the CCM mask showed no obvious transmission dips (Figure 5a). This phenomenon has been interpreted as a Rayleigh−Wood anomaly associated with diffraction,[31] which has also been observed in the case of 2D hollow shell arrays.[29] As can be seen from Figure 5a, the transmission spectra of the nanonets sometimes show more than one dip. For example, in addition to the main dip at 1338 nm, the spectrum of the 1000 nm-nanonet also demonstrated two weak dips centered around 840 and 510 nm, respectively. These multiple transmission dips could be attributed to the higher order diffractions of the nanonet structures. Notably, a linear relationship between the main transmission dip position, that is, the stop band position (λ_d) of the nanonets, and the CCM particle diameter (i.e., the periodic spacing of the nanohole arrays) was found (Figure 5b), which means the λ_d value of the nanonets only depends on the spacing of the nanohole arrays, indicating a nearly constant filling fraction of nanonets with different hole sizes. In addition, the λ_d values of the Ag_2S nanonets calculated by adopting the effective medium estimation were in good agreement with the experimental values, as listed in Table 1, which suggests that the as-prepared high-quality nanonets behaved as typical photonic crystals. It may be noted that all the calculated stop band wavelengths were somewhat larger than the

(29) (a) Landstrom, L.; Brodoceanu, D.; Arnold, N.; Piglmayer, K.; Bauerle, D. *Appl. Phys. A: Mater. Sci. Process.* **2005**, *81*, 911. (b) Gao, Y.; Li, A.; Gu, Z.; Wang, Q.; Zhang, Y.; Wu, D.; Chen, Y.; Ming, N.; Ouyang, S.; Yu, T. *Appl. Phys. Lett.* **2007**, *91*, 031910.

(30) Duan, G.; Cai, W.; Luo, Y.; Sun, F. *Adv. Funct. Mater.* **2007**, *17*, 644.

(31) Palmer, E.; Hutley, M.; Franks, A.; Verrill, J.; Gale, B. *Rep. Prog. Phys.* **1975**, *38*, 975.

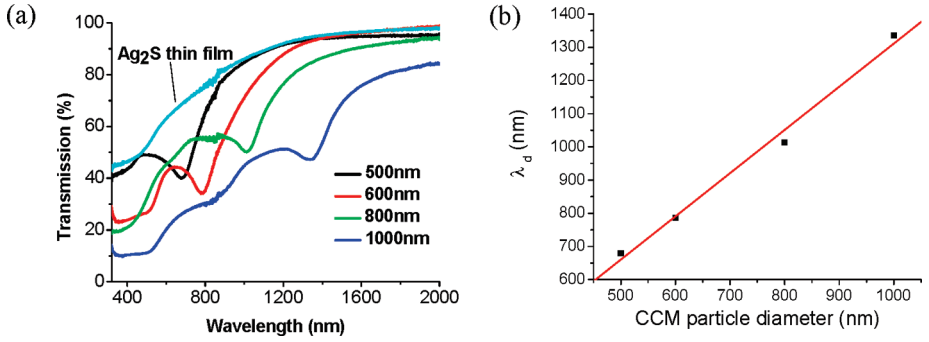

Figure 5. (a) Transmission spectra of Ag_2S nanonets prepared with floating CCMs of different particle diameters as well as unstructured Ag_2S thin films. (b) Linear relationship between the stop band position (λ_d) and the CCM particle diameter.

Table 1. Hole Diameters and Stop Band Positions (λ_d) of Ag_2S Nanonets Masked by CCMs with Different Particle Diameters

particle diameter of CCMs (nm)	hole diameter of Ag_2S nanonets (nm)	λ_d (nm)	
		experimental	calculated
500	400	679	695
600	470	783	842
800	670	1007	1087
1000	800	1338	1390

experimental values, which could be related with the errors in the calculation of the volume fraction of Ag_2S (f_{Ag_2S}) due to the deviation from the perfect geometrical shape. Moreover, a fixed refractive index for Ag_2S (n_{Ag_2S}) was adopted for the approximate calculation, whereas the real refractive index is wavelength-dependent. Furthermore, the current calculation of the stop band wavelength was based on a simplified model for 2D arrays, which could involve some unknown systematic errors for the current 2D nanonets, and hence an improvement in the theoretical calculation of stop band wavelength for 2D nanonets is worthy of further investigation.

Benefiting from the diversity of available gas/liquid interface reactions, this NSL approach at the gas/liquid interface can be easily extended to fabricate large-area ordered nanonets of various materials. When suitable couples of the reactant ion solution and the reactive gas were used (as listed in SITable S1), nanonets of other metal sulfides, metals as well as inorganic minerals could be produced by using analogous experimental procedures. For example, regular nanonets of PbS, Ag, and $CaCO_3$ were readily fabricated (Figure 6). It may be noted that although lots of porous films of inorganic materials including metals and metal oxides have already been produced by CCM templating, it is still difficult to prepare porous films of metal sulfides and inorganic minerals like calcium carbonate by using conventional NSL methods. Moreover, it can be rationally envisioned that multicompositional nanonets may be constructed when a multi-ion solution is employed as the subphase in the current synthetic strategy.

The surface functional groups carried by the CCM mask were found to exert a significant effect on the materials deposition through gas/liquid interface reactions. For example, a CCM mask carrying carboxylic acidic groups, such as the P(St-MMA-AA) CCM, was favorable for the deposition of Ag nanonets while it is difficult to obtain such Ag nanonets by using normal PSt CCM. When the PSt CCM was used as the mask at the gas−liquid interface, only patches of nanoparticles were formed underneath polymer spheres. It has been reported that PSt spheres tended to favor the nucleation of noble metals at the interface between the PSt spheres and the aqueous solution,[23] which could result in the preferential formation of patches of metal nanoparticles underneath polymer spheres. In the case of P(St-MMA-AA) spheres, the surface carboxylate groups could inhibit the nucleation of Ag particles from the solution, thereby favoring the preferential nucleation of Ag particles at the gas−liquid−solid interface, leading to the formation of regular Ag nanonets.

The periodic nanonets may find promising applications in nanofabrication. In this regard, the nanonets can function as a versatile lithographic mask thanks to its regularity and transferability to generate novel periodic nanopatterns on desired surfaces. As a first demonstration, novel gold nanopatterns were fabricated by evaporation deposition with nanonets as the deposition mask. In particular, hexagonally ordered arrays of gold nanoplates were simply produced when a monolayer Ag_2S nanonet was employed as the deposition mask (Figure 7). Furthermore, we demonstrate here a new strategy for metal deposition, which is based on phase-shifting lithography with a bilayer nanonet film as the lithographic mask. The excellent transferability of the present nanonets guaranteed the construction of bilayer nanonets by a layer-by-layer method. Figure 8a shows the SEM image of a typical bilayer Ag_2S nanonet film. When this bilayer Ag_2S nanonet film was used as the deposition mask, novel gold nanoleaf arrays adopting a rectangular order were obtained (Figure 8b). If bilayer nanonets with other different phase shifts were used as the deposition mask, novel gold nanoleaf arrays in a triple-hexagonal order and binary arrays of large and small Au nanoleaves could be obtained (Figure 8c and d). It is noteworthy that nanoarrays in a rectangular order and binary arrays consisting of large and small nanoparticles can be hardly achieved using conventional NSL methods because of the limitation of uniformly sized spheres in a hexagonal order. Another merit of the present lithographic technique to generate nanopatterns lies in its compatibility with nonplanar surfaces due to the flexibility of the nanonet film. Therefore, it may provide us with a new platform to

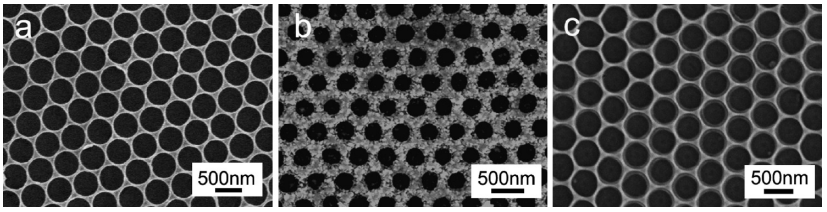

Figure 6. SEM images of PbS (a), Ag (b), and $CaCO_3$ (c) nanonets fabricated by using CCM masks of 500 nm PSt, 450 nm P(St-MMA-AA) and 500 nm PSt, respectively.

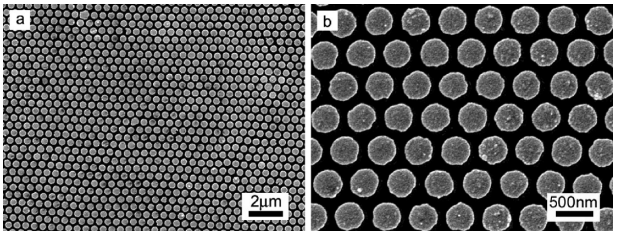

Figure 7. Low (a) and high (b) magnification SEM images of gold nanodisk arrays fabricated by vapor deposition with a monolayer of Ag_2S nanonet (hole diameter ~400 nm) as deposition mask.

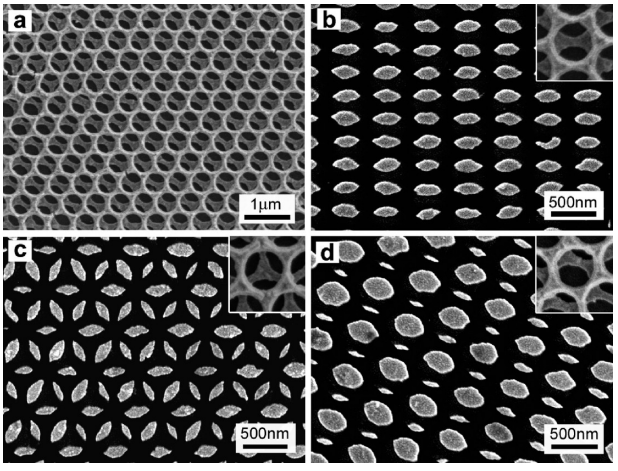

Figure 8. SEM images of a bilayer Ag_2S nanonet film (a) and gold nanopatterns created by evaporation deposition with bilayer Ag_2S nanonets as the deposition masks (b–d). Insets of b–d show the corresponding bilayer nanonets with different phase shifts.

diversify the patterns that can be created by nanosphere lithography.[32–34] The optical properties of the as-fabricated novel patterns of gold nanostructures are currently under investigation, which may find wide applications including light amplification, focusing, and coupling, as well as chemical and biological sensors based on geometry-dependent, local surface plasma resonances (LSPR).[35]

Conclusions

We developed a general nanosphere lithography approach for the facile fabrication of free-standing high-quality nanonets of a variety of inorganic materials in a large scale, which is based on a floating CCM mask at the gas/liquid interface for materials deposition via interfacial reactions. The adjustable CCM masks and controllable reaction conditions allow the production of nanonets with adjustable hole size, spacing, and film thickness. The diversity of gas/liquid interfacial reactions endows the present NSL method with unprecedented compatibility with different kinds of inorganic materials. The as-obtained high-quality nanonets behaved as typical photonic crystals with interesting photonic properties, which may find potential applications as thin film optical sensors. Furthermore, we demonstrated that the obtained transferable, high-quality nanonets can function as versatile lithographic masks to generate novel nanopatterns that are difficult to achieve by using conventional nanosphere lithography route.

Acknowledgment. Financial support from NSFC (Grants 20873002, 20673007, 20633010, and 50821061), MOST (Grant 2007CB936201), and SRFDP (Grant 20070001018) is gratefully acknowledged.

Supporting Information Available: Experimental setup and parameters, additional characterizations of Ag_2S nanonets. This material is available free of charge via the Internet at http://pubs.acs.org.

(32) Haynes, C.; van Duyne, R. *J. Phys. Chem. B* **2001**, *105*, 5599.
(33) (a) Kosiorek, A.; Kandulaski, W.; Chudzinski, P.; Kempa, K.; Giersig, M. *Nano. Lett.* **2004**, *4*, 1359. (b) Kosiorek, A.; Kandulski, W.; Glaczynska, H.; Giersig, M. *Small* **2005**, *1*, 439. (c) Gwinner, M.; Koroknay, E.; Fu, L.; Patoka, P.; Kandulski, W.; Giersig, M.; Giessen, H. *Small* **2009**, *5*, 400.
(34) (a) Zhang, G.; Wang, D.; Möhwald, H. *Angew. Chem., Int. Ed.* **2005**, *44*, 7767. (b) Zhang, G.; Wang, D. *J. Am. Chem. Soc.* **2008**, *130*, 5616.
(35) Zhang, Y.; Reed, J. C.; Yang, S. *ACS Nano* **2009**, *3*, 2412.